

Nonlinear Cascaded Control for a DC-DC Boost Converter

Amirhosein Mansouri¹, Roghayeh Gavagsaz-Ghoachani², Matheepot Phattanasak^{3*}, Serge Pierfederici⁴

^{1,2} Renewable Energy Engineering Department, Shahid Beheshti University, Tehran, Iran

³ Department of Teacher Training in Electrical Engineering, King Mongkut's University of Technology North Bangkok, Bangkok, Thailand

⁴ LEMTA, Université de Lorraine, CNRS, Nancy, France

Email: ¹ amirhos.mansouri@mail.sbu.ac.ir, ² r_gavagsaz@sbu.ac.ir, ³ matheepot.p@fte.kmutnb.ac.th, ⁴ serge.pierfederici@univ-lorraine.fr

* Corresponding Author

Abstract—The Boost Converter is a type of DC-DC converter that operates using switching techniques and is designed to elevate the voltage level. This paper presents a cascaded control for a boost converter to ensure that the inductor current and output capacitor voltage remain in a safe operating zone. Ensuring safe operating conditions and stable closed-loop poles is crucial because it guarantees that both current and voltage remain within the designated operating range. This preventive measure prevents any damage to components like capacitors (C), inductors (L), and switches. Unstable operation, on the other hand, could lead to oscillations and an undesirable increase in the amplitude of current and voltage, posing a risk to all components involved. The research contribution involves an investigation of cascaded control, utilizing power and energy concepts due to their advantageous effects on system performance and design. By implementing nonlinear controllers based on a large-signal averaged model, the closed-loop poles remain independent of operating points, eliminating the need for small-signal linearization. Small-signal linearization makes the controlled system dependent on the operating point. Two controllers are introduced based on power and energy concept, which is easy to understand. The potential practical application of the proposed cascaded control approach is in high-power applications. Tracking the energy stored in the output capacitor is first investigated to validate the proposed control scheme by varying the output voltage reference from 32 V to 50 V. Then, the regulation of the energy voltage is explored by varying the load resistance for the output voltage at 50 V. Both are done using a switched model using MATLAB/Simulink software. Simulation results are given to demonstrate the effectiveness of the proposed method. The key metrics used to assess the effectiveness of the proposed control scheme are the undershoot voltage and robustness. The results show that the studied system's tracking, regulating operations and robustness properties are as expected. The proposed method faces a challenge with the number of sensors required. To address this, observers can be utilized to reduce sensor usage while maintaining measurement accuracy. The proposed method can be applied to other power electronic systems.

Keywords—Control; Nonlinear; DC-DC Converter.

I. INTRODUCTION

A. Significance of Boost Converters

Boost Converter belongs to the category of DC-DC converters that operate based on switching and can increase the voltage level. This converter, also known as a step-up converter, temporarily stores the input energy and then

releases it at the output. In this way, the converter converts a lower DC voltage level to a higher voltage level. Energy storage can occur in magnetic field storage components (inductors) or electric field storage components (capacitors). This process is accomplished using various active or passive switching elements. Power switches belong to the category of active switching elements, while diodes belong to the category of passive switching elements. Boost converter, which is a voltage-level amplifier for DC, has a wide range of applications in various industries such as transportation [1]-[2], renewable energy systems [2]-[5], and household appliances [6].

Different classifications of this converter, such as isolated and non-isolated, unidirectional, or bidirectional, hard-switched, or soft-switched, have been introduced [1], [7]-[21]. The isolated converter typically employs a transformer to ensure galvanic isolation, meeting safety standards, and enabling the adjustment of input/output voltage ratios. Unidirectional and bidirectional converters facilitate power flow in specific directions. While hard-switched converters may experience elevated switching losses, soft-switched converters, employing resonant circuits, can mitigate these losses. With the help of this classic converter, other converters such as three-level boost converters [22]-[28] or interleaved boost converters [29]-[31] have also been introduced.

A generalized state-space average model for multi-phase interleaved converters is discussed [32]. A comprehensive study in transient, steady-state, and switching dynamics is presented. [33] focuses on the analysis and design of a soft-switched clamped-resonant interleaved boost converter. It could be valuable for those interested in soft-switching techniques and resonant converters. A high-gain compact interleaved boost converter specifically designed for photovoltaic (PV) applications is studied in [34]. It addresses the issue of reduced voltage stress. It could be useful for researchers and practitioners working on PV systems. [35] investigates a voltage-mode controller for a DC-DC multilevel boost converter. It could be interesting for those studying multilevel converters and control techniques. A high step-up coupled-inductor cascade boost DC-DC converter with a lossless passive snubber [36]. It could be relevant for



those working on high step-up converters and snubber designs.

B. Control of Boost Converters

There are various control structures available in the literature for regulating a boost converter. One commonly used technique is voltage mode control (VMC), which utilizes a single control loop. However, the boost converter is a non-minimum phase system, and when the inductance and capacitance values are low, the negative zero of the transfer function can cause instability. VMC is typically employed in small power applications. In high-power applications, ensuring the safety of the system requires precise control of the input current. This has led to the popularity of cascaded control structures. These structures consist of an outer voltage loop and an inner current loop. The outer loop regulates the output voltage, while the inner loop controls the input current. By using a cascaded control structure, both the output voltage and input current can be effectively regulated, ensuring safe and stable operation in high-power applications.

Ensuring proper control over the output voltage of a boost converter is crucial, particularly in applications that require the input voltage to remain within an acceptable range ($\pm 10\%$) due to the sensitivity of these specific applications. In [37], some control methods have been compared to each other. The comparison criteria in [37] include the number of control loops and the number of sensors. If there are two control loops, typically the dynamics of the loops are separated [38]-[42]. Reducing the sensors is another important issue in the controllers.

The amount of electric energy generation by a source and its consumption by a load will not be constant at all times. For example, systems that rely on solar energy to generate their electricity can be mentioned. Sometimes, solar panels produce less power due to phenomena such as shading. Also, the consumption of electric energy varies during different hours of the day. Voltage level changes can have irreparable effects on the converter and the load. Therefore, a controller is needed to adjust the voltage level according to new conditions in the shortest possible time. Some controllers, such as proportional-integral (PI) controllers, do not possess this characteristic under all conditions. For this reason, researchers employ nonlinear controllers for this purpose. For the classical PI controller, since it is linearized, its performance is desired around the operating point [43]-[48]. Linearization makes the controlled system dependent on the operating point. The PI controller operates based on predefined characteristics. If these characteristics change, the controller may not perform adequately [49]. One of the limitations of this controller is its inability to respond to external disturbances such as load changes [50].

The indirect sliding mode control (SMC) is a method that has a constant switching frequency compared to the classical sliding mode and does not suffer from chattering [51]-[53]. In practice, implementing switching through the classical sliding-mode controller will not be instantaneous, and there will be an error at the sliding surface level [54]. Therefore, switching occurs with imperfections, leading to an undesirable phenomenon called chattering. Chattering causes high-frequency oscillations in the controller [55]. It appears

as oscillations in the vicinity of the sliding surface. This phenomenon creates a type of persistent mode error and prevents complete alignment with the sliding surface.

SMC has been applied in various applications, such as photovoltaic systems [56] or fuel cells [57]-[59]. Improved methods have been proposed for this control method. For example, in [60], the sliding surface was modified to increase the stability region of the studied system. However, other solutions have also been suggested to avoid instability based on Lyapunov [61]-[65].

Control based on flatness properties is another control method that has many advantages [66]-[72]. The flatness controller has the ability to track a high-level trajectory. It is a robust controller. Another good feature of this controller is the ability to predict system behavior. Its application improves the dynamic response of the system [73]. One of the challenges of this method is the high number of sensors. To overcome this challenge, some variables can be estimated [62], [70]. Considering different studied systems, different control methods [74], and hybridizing with other controllers can be used [75]-[76].

C. Research Contribution

In this paper, two controllers are introduced based on power and energy. These controllers are applied as inner and outer loops on the DC-DC boost converter. Compare to the classical control approach using PI controller, where transfer functions are usually used, the proposed method is more straightforward. In order to regulate the output voltage of a DC-DC converter, such as a boost converter, which refers to the voltage across the output capacitor, one could opt to directly control the voltage. However, when considering the time differential equation for the output capacitor voltage, it becomes apparent that it is influenced by the duty cycle and the input current, resulting in a nonlinear system. An alternative approach involves utilizing the time differential energy equation, where the time variation of the energy under consideration is linearly dependent on the difference between the input and output power. This approach offers a simpler handling of the system.

Since the DC-DC converter is nonlinear, linearization technique using a small signal should apply to make the system linear. Then, a classical approach can be used to place the poles at the desired location on the S-plane. However, linearizing is done for a chosen operating point. It means that the transfer function obtained for the first operating point may not exact for other operating points. Finally, one can find that when the operating point changes, the locations of the poles might move. Contrary to the proposed approach, the transfer function is not necessary if both control loops are well separated.

In this paper, feedback linearization, which refers to discovering a feedback strategy and a coordinate alteration that convert a nonlinear electrical system into a linear and controllable one, is used without small-signal linearization [29], [77]. The feedback linearization controller will be employed in both loops to steer the input power P_i towards its desired value ($P_{i,ref}$) and guide the stored energy in the capacitor, y , towards its desired value (y_{ref}). In situations

where it is necessary to counteract uncertainties in parameters or errors in modeling, the control law resulting from feedback linearization generates a term that facilitates the adjustment of the dynamic behavior for the error convergence, $\varepsilon = y_{ref} - y$ and $\varepsilon = P_{iref} - P_i$, to reach zero. The design of this fictional control is accomplished through the use of a control law. Ultimately, the energy error will asymptotically converge to zero.

The research contribution is to study a cascaded control based on power and energy concepts because of its benefits in the performances, and design. By employing this method, it is ensured that the inductor current and output capacitor voltage of the boost converter remain within a safe operating range. Additionally, the closed-loop poles do not move independently of operating points, thanks to the implementation of nonlinear controllers based on a large-signal averaged model, without resorting to small-signal linearization. After introducing the controller equations, the system under study is implemented in MATLAB/Simulink software. Then, the obtained results are presented using this controller.

D. Organization of Paper

The structure of the article is as follows: after the introduction, the studied converter is introduced in the second part. In addition, the proposed control structure is explained. In the third part, the simulation results for the tracking, regulation, robustness, effect of parameter control and performance comparison are given and finally the conclusion is introduced.

II. METHOD

The method section provides the explanation of the studied system and introduces the control structure for the converter. The first part of method section provides a detailed explanation of the studied system, including the circuit diagram of the boost converter and the symbols used in the analysis. The second part of this section, describes the control structure with the inner power loop and outer energy loop controllers. A flowchart of the research methodology is presented. The derivations and mathematical expressions are presented. The controller equations will be presented step by step for both loops.

A. System Presentation

In this section, the DC-DC boost converter is presented. The circuit diagram of this converter is shown in Fig. 1. The inductor, switch, and diode are the three main components of this converter. The minimal number of elements in this converter achieves the simplicity of design and construction. The inductor is placed on the input side of the converter, and a capacitor can be connected in parallel with the load on the output side.

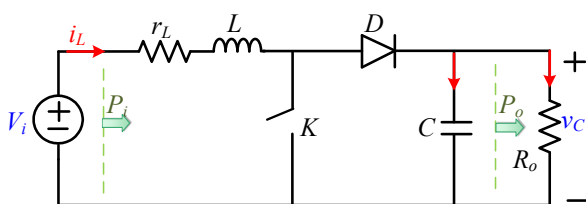


Fig. 1. Circuit diagram of DC-DC Boost converter

The boost converter includes an input voltage source denoted by V_i . The storage elements include an inductor represented by L and a capacitor denoted by C . The load resistance is R_o , and the series resistance of the inductor is r_L . The switching period T and the switching frequency of the system $f_s = 1/T$ are defined. Table I presents the symbols used in the studied system. The symbols for the inductor current (i_L), capacitor voltage (v_c), physical parameters of the converter, and control parameters are introduced.

TABLE I. SYMBOL OF SYSTEM

Description	Symbol
Input voltage	V_i
Inductor	L
Series resistance of the inductor	r_L
Capacitor	C
Load resistance	R_o
Period and switching frequency	T, f_s
Input power	P_i
Current through the inductor	i_L
Voltage across the capacitor	v_c
Switching-command signal	u
Duty cycle	d
Reference value for input power	P_{iref}
Reference value for capacitor voltage	V_{cref}
Energy stored in the capacitor and its reference	y, y_{ref}
Control parameter	ξ
Power loop control parameter	ω_n
Energy loop control parameter	ω_{ny}
Energy loop control parameter	$\omega_{yFilter}$

It is assumed that the boost converter operates in continuous conduction mode (CCM), meaning either the switch or the diode is conducting. Therefore, two operating modes are defined. In the first mode, the switch conducts and the diode is open. In the second mode, the switch is open and the diode conducts. The control signal u is defined as “1” when the switch is closed, and it is defined as “0” when the switch is opened. The symbol of d represents the duty cycle of the switch conduction, which is a part of the switching period.

The inductor current (i_L) and the voltage across the capacitor (v_c) are the state variables of the system. Fig. 2(a) shows the circuit diagram of converter when the command signal $u = 1$. The switch K is close and diode D is open. Fig. 2(b) shows the circuit diagram of converter when the command signal $u = 0$. The switch K is open and diode D is close. Using Kirchhoff's laws, the equations for the loop and node can be written for each mode. By integrating these two operating modes using the control signal, the equations for the converter, which represent the changes in state variables over time, can be obtained. The governing equations of the boost converter can be expressed as equation (1).

$$\begin{cases} \frac{di_L}{dt} = \frac{1}{L}(V_i - r_L i_L - (1-u)v_c) \\ \frac{dv_c}{dt} = \frac{1}{C}\left((1-u)i_L - \frac{1}{R_o}v_c\right) \end{cases} \quad (1)$$

In Table I, the reference value for the input of the control block is P_{iref} . The control parameters such as ξ and ω_n , will be explained in more details in the next section. For the

controlled system, with the second-order response, its behavior can be characterized by a standard form as (2).

$$\frac{C(s)}{R(s)} = \frac{\omega_n^2}{s^2 + 2\xi\omega_n + \omega_n^2} \quad (2)$$

where ξ is the damping coefficient and ω_n is the natural frequency.

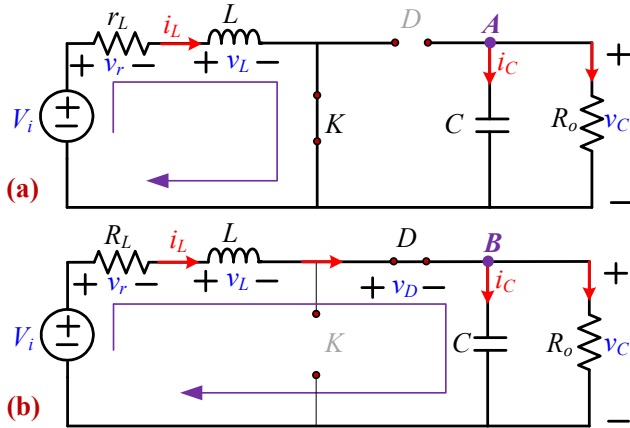


Fig. 2. Circuit diagram of DC-DC Boost converter: (a) The command signal is one, (b) The command signal is zero

Depending on the values of ξ , different modes can be defined for the second-order system. These four modes are shown in Table II. The dynamic behavior of the system is determined by the number and types of poles. The four given modes in the second column can occur. In system design, a desired value of ξ is typically chosen as 0.707.

TABLE II. DIFFERENT MODES IN SECOND-ORDER SYSTEMS WITH VARYING Z (DAMPING FACTOR)

No.	Case	ξ	Poles of C(s)/R(s)	
1	Zero-damped	$\xi = 0$	Two poles	Imaginary
2	Under-damped	$0 < \xi < 1$	Two poles	Complex conjugate
3	Critically-damped	$\xi = 1$	Two poles	Equal
4	Over-damped	$\xi > 1$	Two distinct poles	Negative real and unequal

B. Control System

In this section, the controller equations are introduced. There are two loops for the control section (Fig. 3). The power controller is used as the inner loop to control the input power of the boost converter. The energy controller is used as the outer loop to control the energy stored in the boost converter capacitor.

The objective of this research paper is to design a cascaded controller for a boost converter, with a specific focus on two loops:

- The first loop involves controlling the input power of the boost converter. To accomplish this, an inner power loop controller will be used.
- The second loop relates to controlling the energy stored in the capacitor of the boost converter. In this case, an outer energy controller will be implemented.

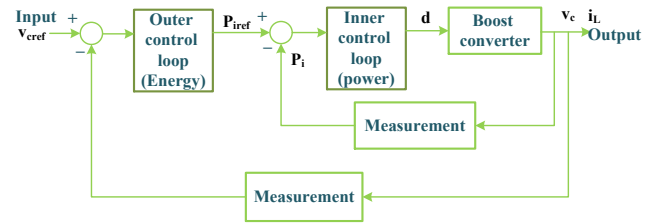


Fig. 3. Cascaded control structure consists of inner power loop and outer energy loop

1) Inner Power Loop

In this section, the power controller equations for the boost converter are introduced. The input power to the converter is denoted as P_i . Its relationship is given by the product of the input current and input voltage, as shown in equation (3).

$$P_i = V_i i_L \quad (3)$$

The derivative of the input power, \dot{P}_i , can be obtained in general form as shown in equation (4).

$$P_i = V_i \cdot i_L \Rightarrow \dot{P}_i = V_i \frac{di_L}{dt} + i_L \frac{dV_i}{dt} \quad (4)$$

If the input voltage is considered constant, its changes become zero. Therefore, a term is eliminated in the derivative of input power equation. Hence, equation (4) can be written as (5).

$$P_i = V_i \cdot i_L \Rightarrow \dot{P}_i = V_i \frac{di_L}{dt} \quad (5)$$

In equation (5), the changes in the inductor current with respect to time are observed. This expression is one of the governing equations for the boost converter. But it is transformed into a large-signal averaged model with the continuous duty cycle d . The changes in this state variable are recalled in equation (6).

$$\frac{di_L}{dt} = \frac{1}{L}(V_i - r_L i_L - (1-d)v_c) \quad (6)$$

Using equation (6) and substituting it into equation (5), we can write equation (7).

$$\dot{P}_i = \frac{V_i}{L}(V_i - r_L i_L - (1-d)v_c) \quad (7)$$

Using equation (3) and equation (7), one can write (8).

$$\frac{L \dot{P}_i}{V_i} = V_i - r_L \frac{P_i}{V_i} - v_c + d v_c \quad (8)$$

Now, the duty cycle d can be obtained as (9).

$$d = \frac{L \dot{P}_i}{V_i v_c} + \frac{r_L P_i}{V_i v_c} + 1 - \frac{V_i}{v_c} \quad (9)$$

Note that the obtained duty cycle is for a static operating point. The control block diagram is shown in Fig. 4.

The controller with feedback linearization [28], [77] is used to drive the input power P_i towards its reference value (P_{i_ref}). Its control equation is given by (10).

$$\dot{P}_i - \dot{P}_{i_ref} + K_1(P_i - P_{i_ref}) + K_2 \int (P_i - P_{i_ref}) = 0 \quad (10)$$

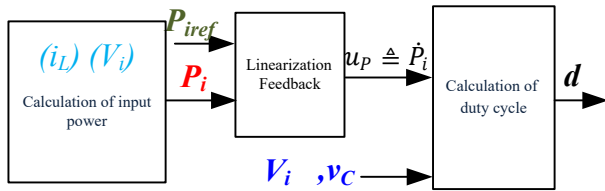


Fig. 4. Power control loop to calculate the duty cycle of the boost converter

Therefore, P_i is obtained according to equation (11).

$$u_p \triangleq \dot{P}_i = \dot{P}_{iref} + K_1(P_{iref} - P_i) + K_2 \int_0^t (P_{iref} - P_i) d\tau \quad (11)$$

In this equation, the control coefficients are defined as (12).

$$K_1 = 2 \xi \omega_n, K_2 = \omega_n^2 \quad (12)$$

where ξ is the damping coefficient and ω_n is the natural frequency.

The integral term compensates the model errors. Hence, a zero static error can be guaranteed in the steady state. This equation comprises the errors $\varepsilon = P_{iref} - P_i$ between the input power, and its reference verifies the second-order equation (13).

$$\ddot{\varepsilon} + k_1 \dot{\varepsilon} + k_2 \varepsilon = 0 \quad (13)$$

The optimum values corresponding to $p(s)$ taken from (13) to a desired characteristic polynomial (Eq. (14)). This optimum choice can be got by design root locations.

$$p(s) = s^2 + 2\zeta\omega_n s + \omega_n^2 \quad (14)$$

Consequently, the gain parameters are achieved by finding between (13) and (14).

By substituting equation (11) into equation (9), the output of the controller, which is the duty cycle, is obtained as (15).

$$d = \frac{L u_p}{V_i v_c} + \frac{r_L P_i}{V_i v_c} + 1 - \frac{V_i}{v_c} \quad (15)$$

2) Outer-energy Loop

In the outer loop of the boost converter control, the energy control equations are introduced. This is an external control loop for the converter that controls the output voltage. In the inner current control loop, the control is indirectly performed using the input power. Therefore, the output of the outer loop can serve as a reference input for the inner loop.

According to the boost converter circuit shown in Fig. 1, the input power to the converter is denoted as P_i . Its relationship is given by equation (16).

$$P_i = V_i i_L \quad (16)$$

The output power of the converter, p_o , can be expressed as equation (17).

$$p_o = v_c i_o \quad (17)$$

The energy stored in the output capacitor can be represented by equation (18).

$$y = \frac{1}{2} C v_c^2 \quad (18)$$

The reference stored energy in capacitor C can be expressed as equation (19).

$$y = \frac{1}{2} C V_{cref}^2 \quad (19)$$

Where v_{cref} is the reference output voltage.

The rate of change of stored energy in the capacitor with respect to time is given by equation (20).

$$\dot{y} = \frac{dy}{dt} = P_i - p_{loss} - p_o \quad (20)$$

Neglecting losses ($p_{loss} = 0$), the previous equation (20), can be written as (21).

$$P_i = \dot{y} + p_o \quad (21)$$

The controller using the feedback linearization technique [28], [77], [78], [79] is used to drive the stored energy in the capacitor, y , towards its reference value (y_{ref}). In addition, in regulating the stored energy when disturbances occur. The control equation is given by equation (22).

$$\dot{y} - \dot{y}_{ref} + K_{1y}(y - y_{ref}) + K_{2y} \int_0^t (y_{ref} - y) d\tau = 0 \quad (22)$$

Note: Neglecting losses, the model is simple to demonstrate how to implement the proposed controller. Indeed, since the model is inexact, the controller with an integral term can be used to deal with this issue. With neglecting p_{loss} , the steady-state error exists. The integral term of the controller ($\int (y - y_{ref}) dt$) is used to address and eliminate static error in the control system. The integral term helps to correct for any long-term imbalances or biases in the system. It provides a feedback mechanism that ensures the control system reaches and maintains the desired setpoint, even in the presence of external disturbances or system uncertainties. Therefore, the proposed controller can handle the inexactness of the model in practical situations.

Therefore, using the previous equation (22), \dot{y} can be obtained as (23).

$$\dot{y} = \dot{y}_{ref} + K_{1y}(y_{ref} - y) + K_{2y} \int_0^t (y_{ref} - y) d\tau \quad (23)$$

In the linearization feedback equation, the control coefficients are defined as follows in (24).

$$K_{1y} = 2 \xi \omega_{ny}, K_{2y} = \omega_{ny}^2 \quad (24)$$

where ξ is the damping coefficient and ω_{ny} is the natural frequency.

By substituting equation (23) into (21), the output of the controller, which is the input power, can be obtained as (25).

$$P_i = \dot{y}_{ref} + K_{1y}(y_{ref} - y) + K_{2y} \int_0^t (y_{ref} - y) d\tau + p_o \quad (25)$$

The inner loop has faster dynamics than the outer loop. Therefore, the control parameter ω_{ny} is selected at least ten times smaller ($\omega_{ny} \leq \frac{\omega_n}{10}$) in power energy control. The inner loop control parameter $\omega_n = \frac{2\pi f_s}{20} = 3000$ rad/s is selected. The outer loop parameter $\omega_{ny} = \frac{\omega_n}{10} = 300$ rad/s is selected.

The control block diagram is shown in Fig. 6. The output of this outer loop is the reference input for the input power. In this outer loop, the output voltage can be controlled by controlling the stored energy in the capacitor.

To avoid the higher current peak of the output capacitor during changing the output voltage reference, for example, during startup, a second order filter is used to smooth the energy reference to meet the requirements of the maximum peak current for the system.

The energy reference is planned with a dynamic as a second order system without overshoot (damping factor $\xi = 1$). Therefore, the transfer function of the second order filter is expressed as (26).

$$\frac{y_{ref}(s)}{y_{ref}^*(s)} = \frac{\omega_{yFilter}}{(s + \omega_{yFilter})^2} \quad (26)$$

The angular frequency $\omega_{yFilter}$ related to the time constant τ as defined in (27).

$$\tau = \frac{1}{\omega_{yFilter}} \quad (27)$$

The time response with a step function of the reference y_{ref} is given by (28) [80].

$$y_{ref}(t) = \frac{1}{\tau} \left(e^{-\frac{t}{\tau}} y_{ref,init} (t + \tau) - y_{ref,final} \left(t e^{-\frac{t}{\tau}} + \tau \left(e^{-\frac{t}{\tau}} - 1 \right) \right) \right) \quad (28)$$

Suppose that the energy stored in the output capacitor $y_{ref}(t)$ tracks well its reference thanks to the proposed controller, the capacitor current can be derived from (29).

$$i_c(t) = C \frac{dv_c}{dt} \quad (29)$$

with $v_c = \sqrt{\frac{2y_{ref}}{C}}$. Then, the capacitor current can be expressed as (30).

$$i_c(t) = \frac{1}{\tau} \left(y_{ref,init} \cdot e^{-\left(\frac{t}{\tau}\right)} - \frac{y_{ref,init} \cdot e^{-\left(\frac{t}{\tau}\right)} \cdot (\tau + t)}{\tau} + \frac{t \cdot y_{ref,final} \cdot e^{-\left(\frac{t}{\tau}\right)}}{\tau} \right) \quad (30)$$

From the parameters of the studied system, the capacitor current $i_c(t)$ is plotted with different time constant τ in Fig. 5. It can be seen that the required maximum peak current of the capacitor can be respected by adjusting the value of τ . For

the given capacitance, the time constant τ can be determined by the requirement. For this paper, the value of the time constant is chosen as $\tau = 10$ ms, therefore, $\omega_{yFilter} = 100$ rad/s.

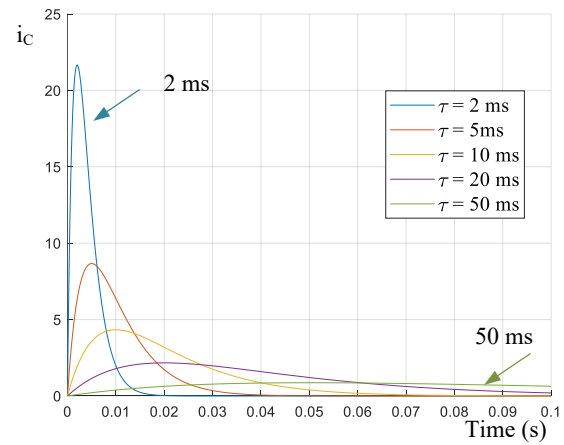


Fig. 5. Capacitor current response with step input for different time constant τ

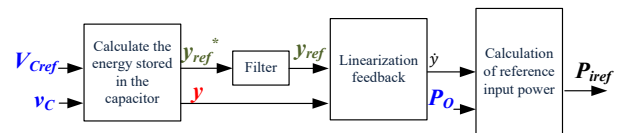


Fig. 6. Outer energy control loop, it calculates the input power reference for the inner power loop of the boost converter

Note: The electromagnetic energy stored in the inductor is assumed to be negligible compared to the electrostatic energy stored in the capacitor. Therefore, electromagnetic energy is not considered in the power balance equations. As a summary, Fig. 7 shows the flowchart of the research methodology. The steps performed are listed in order. The studied system consists of a converter and its control section.

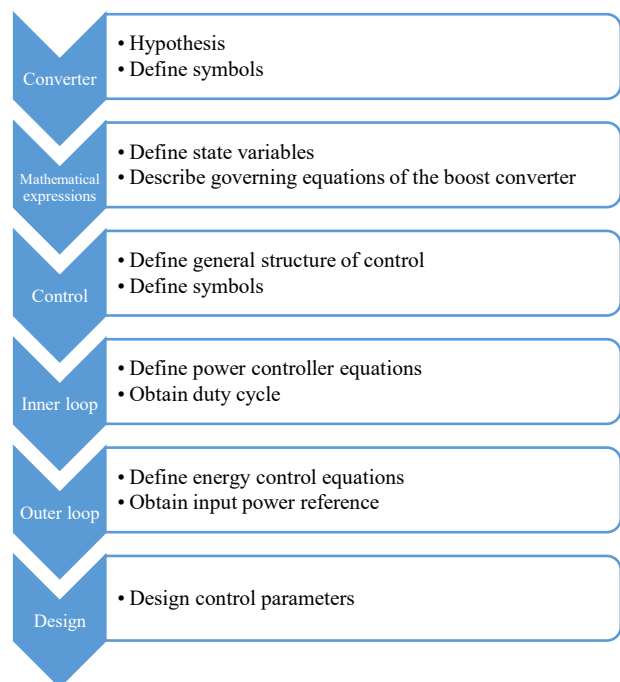


Fig. 7. Flowchart of the research methodology

The governing differential equations of the boost converter are derived using Kirchhoff's voltage and current laws. These laws are written for two states: when the switch is open or closed, based on the circuit configuration of the converter. The control signal determines the state of the switch, whether it is open or closed. The duty cycle value is calculated by the control section.

A cascade controller is proposed, which consists of an outer loop and an inner loop. The outer loop is the capacitor energy control loop, which can effectively control the output voltage. The inner loop is the input power control loop, which can control the input current. The dynamics of the energy (voltage) control loop are slower compared to the power (current) control loop, and this point is taken into account when determining the bandwidth of each loop for design purposes.

The mathematical equations of each loop, along with the control block diagram, are introduced. At the input of the control section, the reference value of the output voltage is provided to the outer loop. The output of this loop generates the reference input power. This value is fed into the inner loop, and its output is the duty cycle. By using pulse-width modulation (PWM), the duty cycle (d) is converted into a control signal (u). This control signal is applied to the converter.

With the introduced equations, the studied system can be simulated, and the waveforms can be analyzed. In the following, the results obtained from the simulation will be presented.

III. SIMULATION RESULTS

The studied system includes a converter and a control section simulated using MATLAB/Simulink software.

For the control section, the computed duty cycle in equation (15) is utilized. The system consists of a boost converter and a controller. It is assumed that the reference value and system parameters are defined. The controller generates the duty cycle. This duty cycle needs to be transformed into a switching-command signal, which is achievable through pulse-width modulation. Then, the two equations governing the system implemented in MATLAB/Simulink is used to obtain the state variables.

In Table III, the parameters used in the studied system are provided.

TABLE III. PARAMETERS OF THE STUDIED SYSTEM

Parameters	Value
V_i	12 V
L	370 μ H
r_L	0.1
C	100 μ F
R_o	17
f_s	10 kHz
V_{cref}	32, 50 V
ξ	0.707
ω_n	3000
ω_{ny}	300
$\omega_{yFilter}$	100

In this section, the waveforms of the system are presented. The results are shown for variations in the reference voltage of the capacitor and the load resistance. In the first case, the waveforms are investigated for incremental changes in the reference voltage. In the second case, both increases and decreases in the load value are studied.

Then, the performance of the system under input voltage variation is investigated. The influence of control parameter will be presented.

A comparison is performed between the proposed control method and the classical cascaded PI control. The robustness analysis under varying inductance and capacitance is presented. Finally, a discussion is presented.

A. Tracking: Changes in the Output Reference Voltage

Using a Step block, the output reference voltage can be changed at a desired time. For example, the reference voltage is changed from 32 to 50 V at $t = 0.25$ s. The waveforms of the inductor current and the voltage across the capacitor are shown in Fig. 8 and Fig. 9, respectively. The current and voltage settle to their final values after the transient regime.

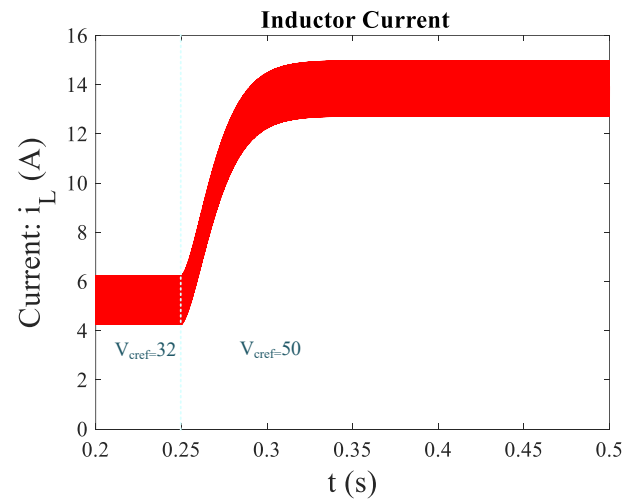


Fig. 8. Variations of the inductor current with respect to time when the output reference voltage changes at $t = 0.25$ s

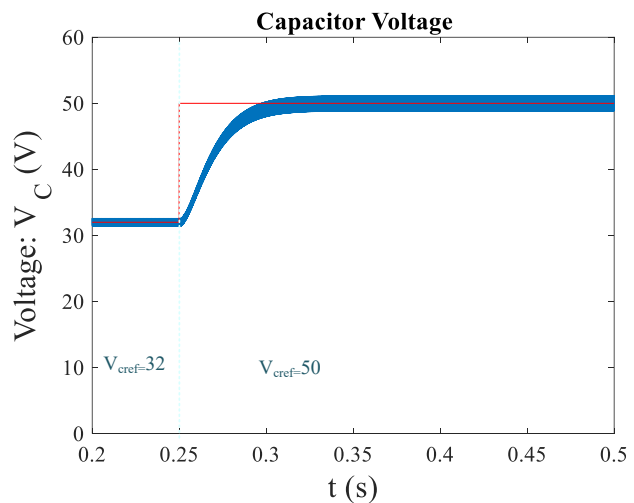


Fig. 9. Variations of the capacitor voltage with respect to time when the output reference voltage changes at $t = 0.25$ s

In Fig. 10, before and after applying the voltage step, the waveforms are magnified. In both cases, the output voltage reaches its reference value in the steady state.

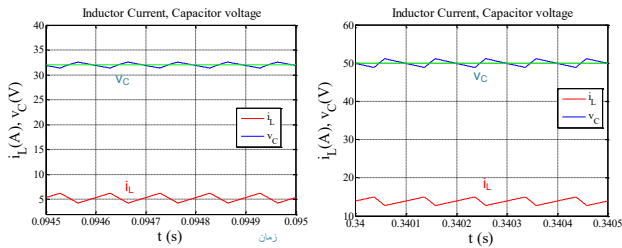


Fig. 10. Variations of the capacitor voltage with respect to time when the output reference voltage changes at $t = 0.25$ s

Fig. 11 illustrates the variations of the energy stored in the capacitor along with its reference.

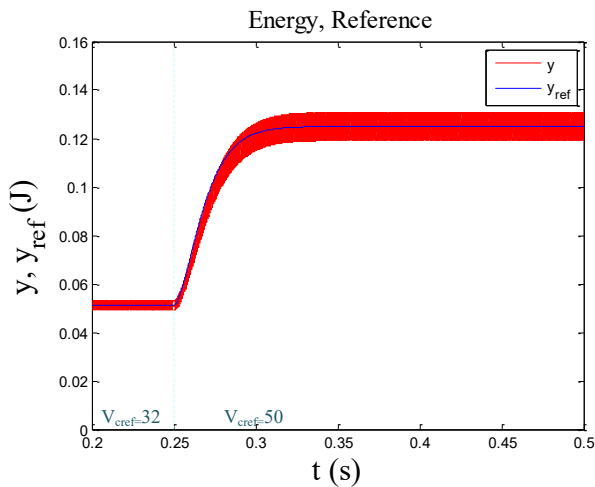


Fig. 11. Variations of the energy stored in the capacitor and its reference with respect to time when the output reference voltage changes at $t = 0.25$ s

According to this figure, the capacitor energy has well followed its reference value. Fig. 12 displays the variations of the input power along with its reference. It can be observed that the input power has effectively tracked its reference value.

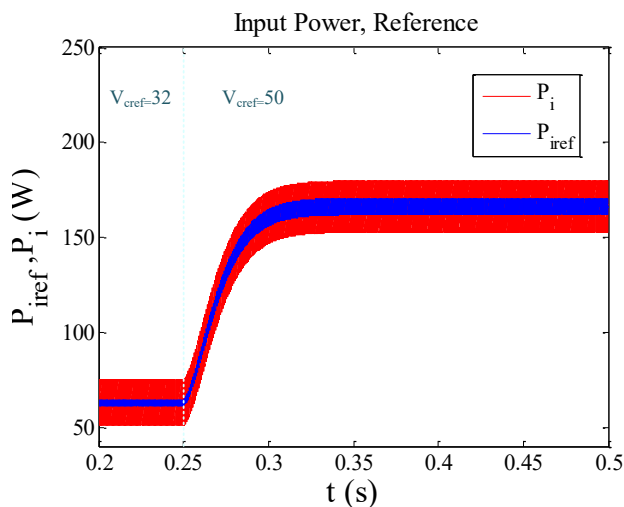


Fig. 12. Variations of the input power and its reference when the output reference voltage changes at $t = 0.25$ s

B. Regulation

Changes in the load resistance are examined in this section to evaluate the controller's performance. Similar to the previous cases, the value of the load resistance can be changed at a desired time using a step input.

1) Decreasing the load resistance

In one example, the value of the load resistance is halved at $t = 0.3$ s. Fig. 13 depicts the waveform of the energy stored in the capacitor and its reference. Fig. 14 shows the waveforms of the inductor current and capacitor voltage.

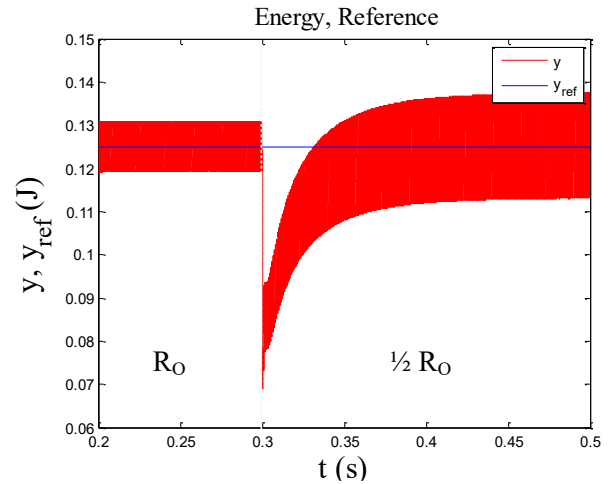


Fig. 13. Energy stored in the capacitor and its reference when the load resistance is halved at $t = 0.3$ s

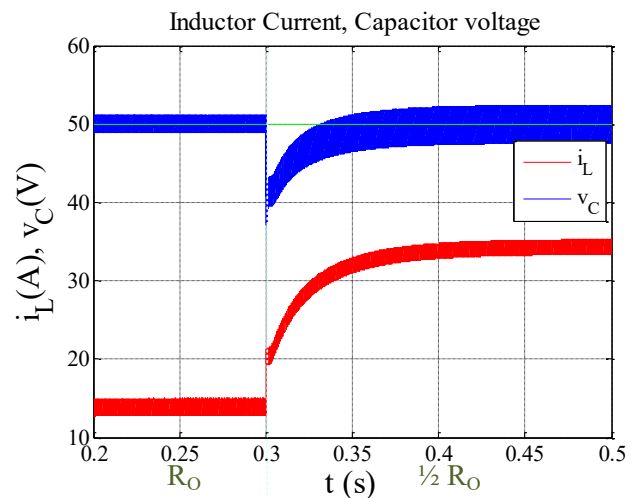


Fig. 14. Inductor current and capacitor voltage when the load resistance is halved at $t = 0.3$ s

When the resistance changes, there is the disturbance on the energy stored in the capacitor, but the controller can reject this disturbance in a finite time corresponding to the chosen control parameters (ω_n, ξ) . Due to the control of the stored energy in the capacitor, the capacitor voltage remains unchanged in steady-state despite the decrease in the load resistance.

Fig. 15 illustrates the variations of the input power and its reference. It can be observed that the controller effectively regulates the power despite the disturbance.

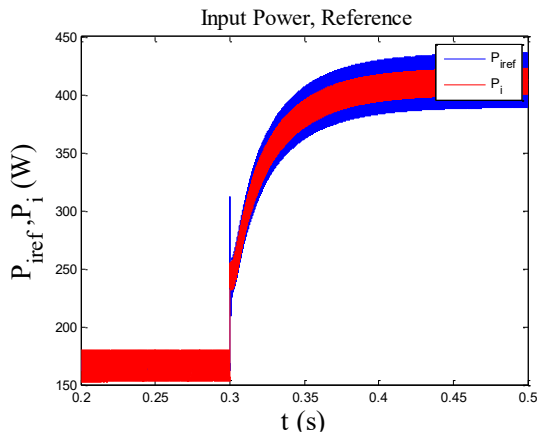


Fig. 15. Variations of the input power and its reference when the load resistance is halved at $t = 0.3$ s

2) Increasing the Load Resistance

In another example, the waveforms of the inductor current and capacitor voltage are shown for a 50% increase in the load resistance in Fig. 16. In this case, the inductor current decreases while maintaining a constant output voltage.

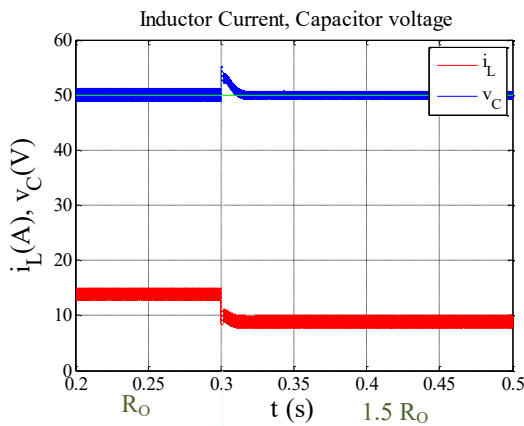


Fig. 16. Inductor current and capacitor voltage for a 50% increase in the load resistance at $t = 0.3$ s

Fig. 17 displays the waveform of the energy stored in the capacitor and its reference, and Fig. 18 illustrates the variations of the input power and its reference. Once again, the controller demonstrates successful power regulation despite the disturbance.

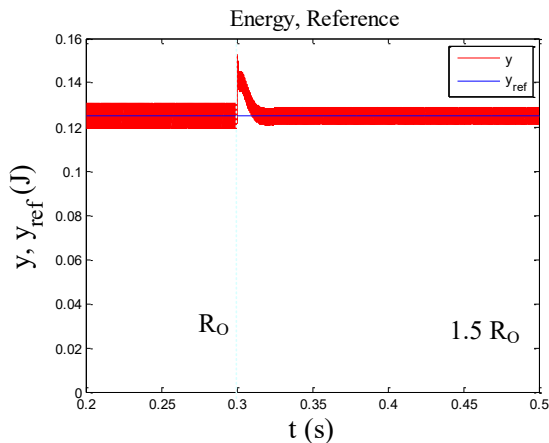


Fig. 17. Energy stored in the capacitor and its reference when the load resistance is increased by 50%

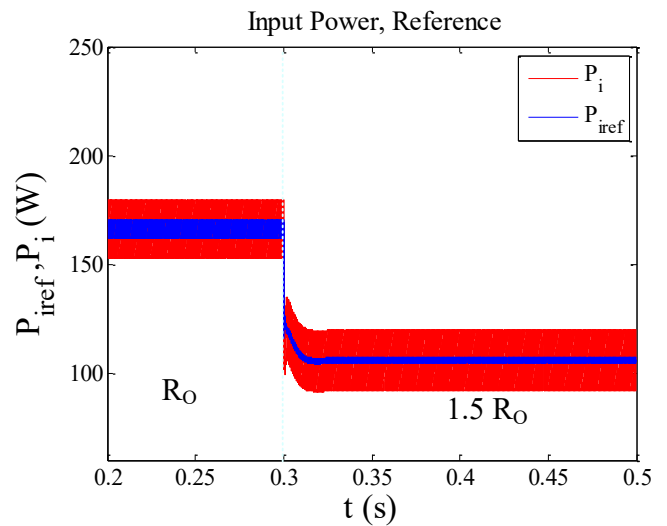


Fig. 18. Variations of the input power and its reference when the load resistance is increased by 50%

C. Performance Investigation Under Input Voltage Variation

Performance of the system could be studied under varying operating conditions. In this section, behavior of the system under varying input voltage is investigated.

The input voltage is changed in two scenarios: one using a step function to alter the input voltage magnitude and another time using a sinusoidal waveform. The waveforms of the studied system are introduced, and the behavior of the system is examined.

Fig. 19 presents the inductor current and capacitor voltage under varying input voltage as step voltage from its nominal value to 10% while other parameters are fixed.

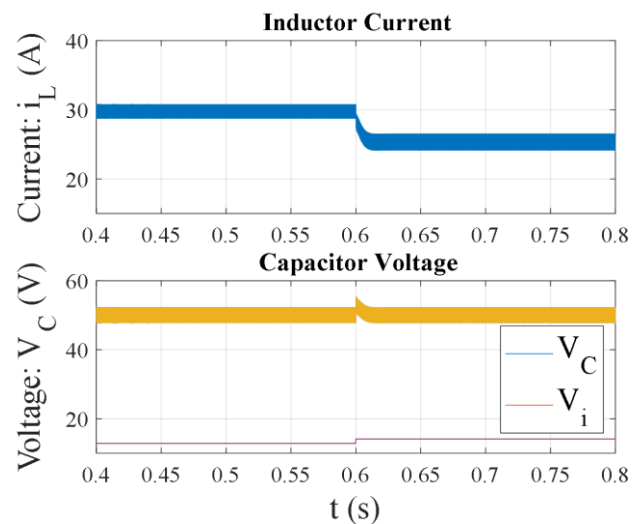


Fig. 19. Inductor current and capacitor voltage for an input voltage variation

Fig. 20 presents the inductor current and capacitor voltage under varying input voltage as $v_i(t) = 2V_i + 1.2\sin(20\pi t)$ while other parameters are fixed. The controllers can reject the disturbance according to Fig. 19 and Fig. 20. Therefore, the output voltage is kept constant.

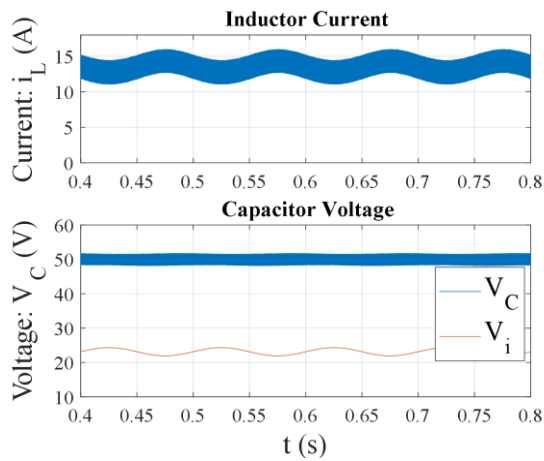


Fig. 20. Inductor current and capacitor voltage for a variation of input voltage with a sinusoidal waveform

D. Influence of Control Parameters

This section examines the effect of control parameters on the system.

The inner loop control parameter ω_n is varied for different simulations. As mentioned previously, the inner loop has faster dynamics than the outer loop. Therefore, the outer loop parameter $\omega_{ny} = \frac{\omega_n}{10}$ rad/s is selected. A load step from R_o to $\frac{R_o}{2}$ at $t = 0.25$ s. The inductor current and capacitor voltage are presented in Fig. 21 and Fig. 22 for the variations of control parameters ω_n and ω_{ny} . It is observed that, increasing the natural frequencies (ω_n and ω_{ny}), makes the dynamics of the system faster. However, in this paper, the value of the inner loop control parameter ω_n is chosen as $\omega_n = 3000$ rad/s to avoid problems with interference noise in practical case.

The inductor current and capacitor voltage during startup are presented in Fig. 23 and Fig. 24 for the variations of cutoff frequency for the energy filter $\omega_{yFilter}$. It is observed that, decreasing the cutoff frequency of the energy filter, makes the dynamics of the system in case of changing the output voltage reference slower. In other words, it does not affect the system's dynamics if the output voltage reference is constant. In this paper, $\omega_{yFilter} = 100$ rad/s is chosen.

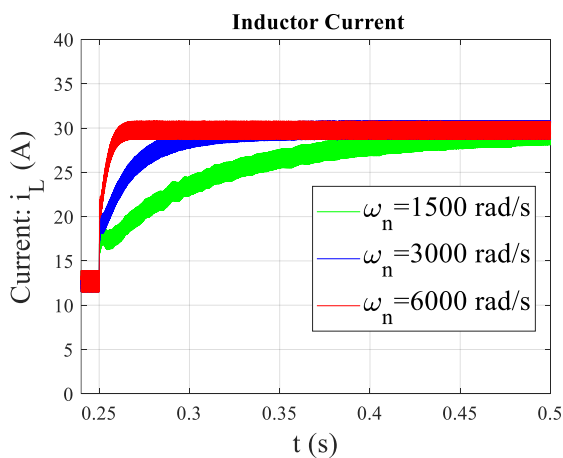


Fig. 21. Inductor current waveforms when the load resistance is reduced at $t = 0.25$ s for different control parameters of the inner and outer loop

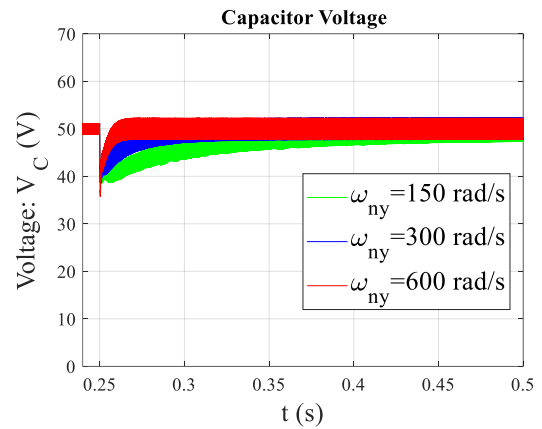


Fig. 22. Capacitor voltage waveforms when the load resistance is reduced at $t = 0.25$ s for different control parameters of the inner and outer loop

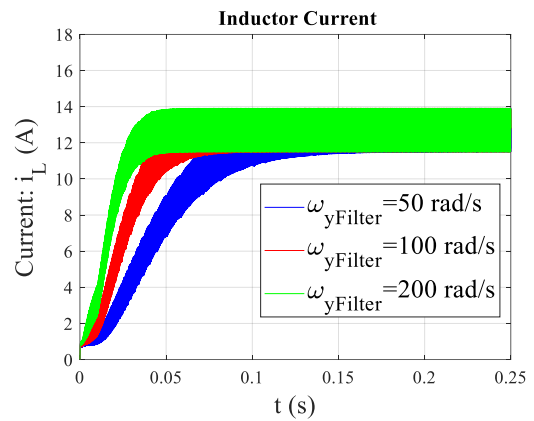


Fig. 23. Inductor current waveforms during startup when cutoff frequency of the energy filter $\omega_{yFilter}$ is varied

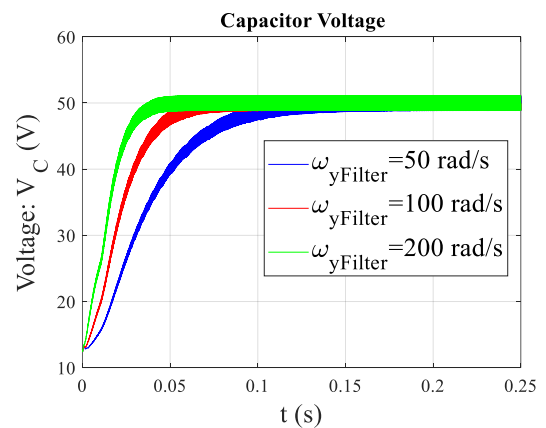


Fig. 24. Capacitor voltage waveforms during startup when cutoff frequency $\omega_{yFilter}$ of the energy filter is varied

E. Comparison of the Proposed Method with the Classical Approach

In this section, a comparison is made between the proposed control method and the classical cascaded PI control. Two PI loops are considered: an inner loop that controls the inductor current and an outer loop that controls the output voltage. The waveforms of the studied system are depicted and analyzed.

Both controllers are designed to achieve the same controlled crossover frequencies for both inner and outer

loops, set at 3000 rad/s and 300 rad/s, respectively. The inner loop of the PI controller exhibits a damping factor $\xi \approx 0.707$ (phase margin = 45 degrees), while the outer loop has phase margin = 70 degrees.

The PI controller is configured with a designated operating point at $V_{oref} = 50\text{ V}$ and a load resistance of $R_o = 8.2\ \Omega$. Notably, both systems demonstrate stable operation. Table IV presents the percentage of undershoot voltage for various output voltage references. It is important to highlight that the undershoot voltage is influenced by the capacitance value and the controlled bandwidth of the controller.

TABLE IV. UNDERSHOOT VOLTAGE FOR DIFFERENT OUTPUT VOLTAGES

$V_{oref}(V)$	Undershoot voltage (%); $\varepsilon = \frac{V_{oref}-v_o}{V_{oref}} 100\%$	
	PI	Proposed
55	30.36	25.2
50	28.56	23.04
40	23.92	17.7
30	20.00	13.4
24	17.16	10.75

As stated in this paper, the capacitance value is relatively small, leading to the anticipation of a significant undershoot voltage. Regarding the undershoot voltage, the system with the proposed controller outperforms the PI controller across all presented results. This is attributed to the proposed controller's ability to leverage knowledge of the output power, allowing it to respond more swiftly compared to the PI controller, where the load power does not feed back to the controller.

Robustness analysis could be employed to show how the system behaves under varying values of the system's parameters. In this section, the robustness characteristic of the system under varying L, C parameters are investigated.

In Fig. 25 and Fig. 26, the inductor current and capacitor voltage are presented when the inductance (L) value is varied. In the first scenario, the inductance is set to 100% of its nominal value, while keeping other parameters fixed. In the second scenario, the inductance is set to 180% of its nominal value using the same methodology.

In the initial scenario, both systems demonstrate robustness. However, in the subsequent case, the system equipped with the PI controller proves to be inadequate in dealing with variations in inductance. In contrast, the system employing the proposed controller exhibits robust performance in the face of such variations.

In Fig. 27, the inductor current and capacitor voltage are presented when the capacitance (C) value is varied. The capacitance is set to -50% of its nominal value, while keeping other parameters fixed. For this point, both systems demonstrate robustness.

It should be noted that compared to the classical cascaded control scheme using PI controller with a small-signal model, using only a current sensor for the inductor current and another voltage sensor for the output voltage can be tuned for better performance for a specific operation point. However, as the location of the pole's changes, the dynamic

performance might change. But it is not the case for the proposed method.

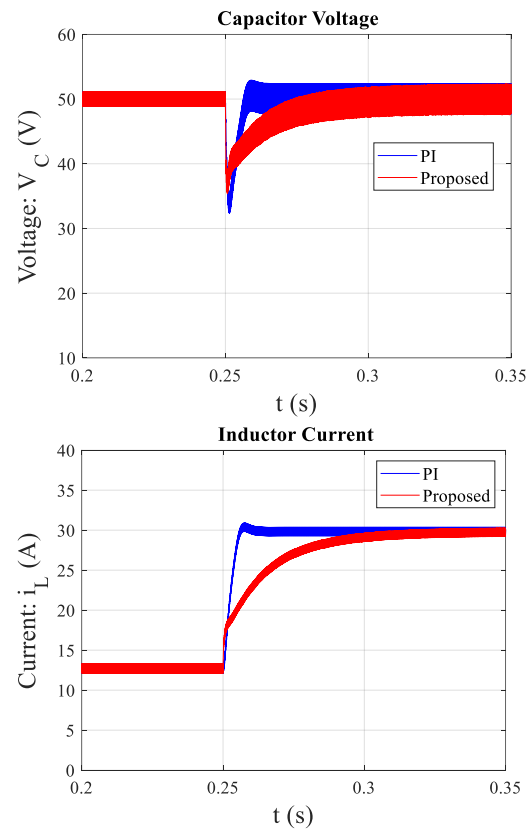


Fig. 25. Inductor current and capacitor voltage for a variation of inductance 100% of its nominal value

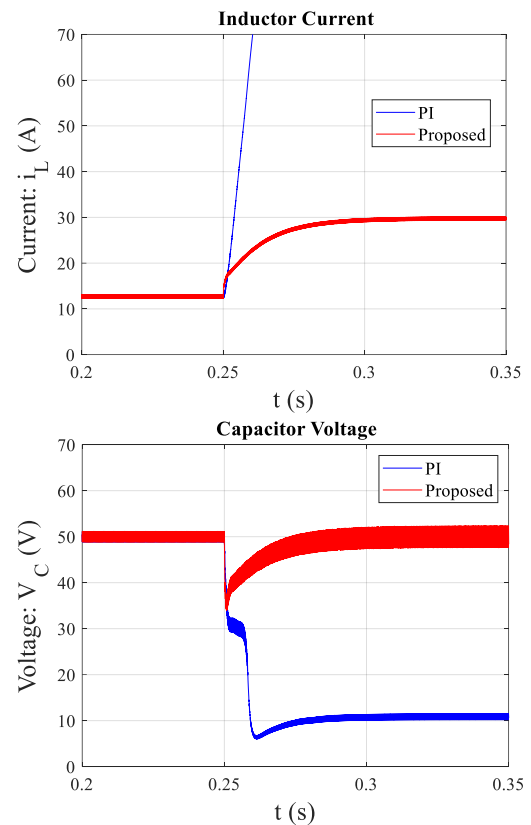


Fig. 26. Inductor current and capacitor voltage for a variation of inductance 180% of its nominal value

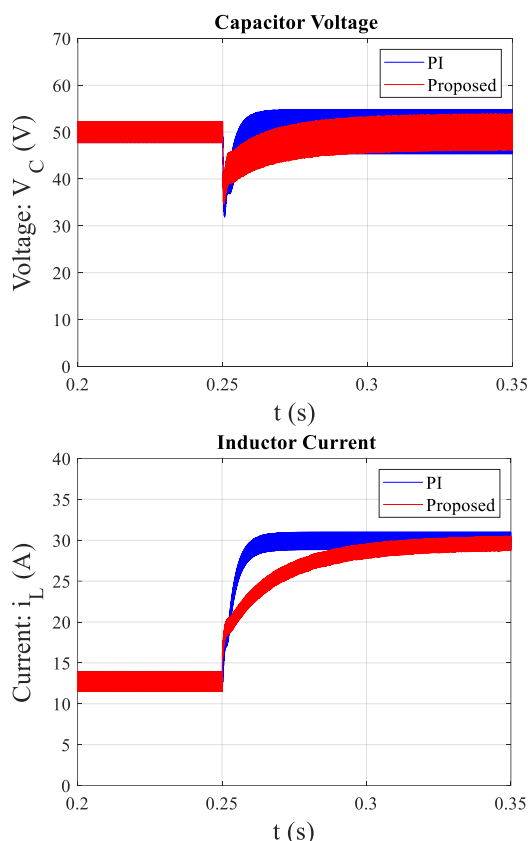


Fig. 27. Inductor current and capacitor voltage for a variation of capacitance -50% of its nominal value

F. Discussion

Tracking and regulation analysis was performed using MATLAB/Simulink software. It demonstrated that the capacitor energy tracks its reference value accurately during an increase in energy reference. To evaluate the control controller's regulation capability, the load resistance was initially increased by 50%. The results showed that energy regulation and consequently voltage adjustment followed this change accurately. In the simulation, the power controller was able to achieve similar results. Additionally, a 50% decrease in load resistance demonstrated the regulation characteristic of the control controller. The practical implementation of this cascaded control can be easily performed for DC-DC converters like the boost converter and can be utilized in various applications of this converter.

The limitation and potential challenges associated with the proposed method are the number of sensors. It can be reduced using observers.

As future work, experimental results can be included. Experimental validation of the proposed control on a prototype boost converter will enhance the practical applicability of the research in real-world applications.

Control of converters is important in photovoltaic systems and fuel cells. Both systems require voltage level increase, and the boost converter performs this task. Furthermore, one of the methods in the field of hydrogen supply as a clean fuel or for energy storage is water electrolysis. This method requires a low voltage level. Therefore, a converter like a

buck converter is needed. The control method can be applied to other power electronic systems and converters.

When analyzing the efficiency of switching power converters, it is crucial to examine both their steady-state and transient performance. While a control approach might be efficient during steady-state operation, it may face difficulties when dealing with transient conditions. However, it is common practice to evaluate the efficiency of switching power converters primarily under steady-state conditions [81]-[83].

IV. CONCLUSION

In this article, in the first step, the relationships related to a power controller were introduced. This controller was applied to a boost converter. The input power was calculated considering the current passing through the inductor and the input voltage of the converter. Then, the power derivative was given. By doing this, the variations in the inductor current appeared, and the governing equation for the boost was replaced by this relationship for the current variations. This revealed the duty cycle relationship, which can be easily extracted.

To ensure that the measured input power follows the reference power, a linearizing feedback controller was used. The control equation includes an integral and derivative terms. Thus, the required power derivative was obtained in the duty cycle formula.

In the second step, the relationships related to an energy controller were introduced. The energy stored in the boost converter capacitor was calculated considering the output voltage of the converter. A second-order filter was employed after the output to utilize the reference value of capacitor energy for proper operation. To ensure that the measured energy follows the reference value well, a linearizing feedback controller was utilized. By using the output power and the energy stored in the capacitor, the reference value of input power can be generated.

The system simulation, including the non-ideal boost converter and the controllers, was performed in the MATLAB/Simulink software environment.

To examine the performance of the controllers, tracking and regulation were demonstrated. In the tracking evaluation, the reference value of energy stored in the output capacitor increased, and the measured capacitor energy was able to follow its reference value well. In the regulation simulation, the load resistance decreased and then increased. The controller effectively performed energy adjustment and, consequently, output voltage regulation in both cases. Similarly, the power controller performed well in both tracking and power regulation scenarios.

The effect of control parameters on the system is investigated. Increasing the natural frequencies for inner and outer loops (ω_n and ω_{ny}), makes the dynamics of the system faster. It is evident that reducing the cutoff frequency of the energy filter ($\omega_{yFilter}$) results in slower system dynamics when there are changes in the output voltage reference.

The behavior of the system under varying the input voltage is investigated. The controlled system can reject the variations of the input voltage.

In terms of undershoot voltage, the system utilizing the proposed controller demonstrates superior performance compared to the PI controller in all the presented results.

The robustness characteristic under variations of inductance and capacitance values is investigated. According to the obtained results, the proposed controlled system is robust. The key results of the proposed method are summarized in Fig. 28.

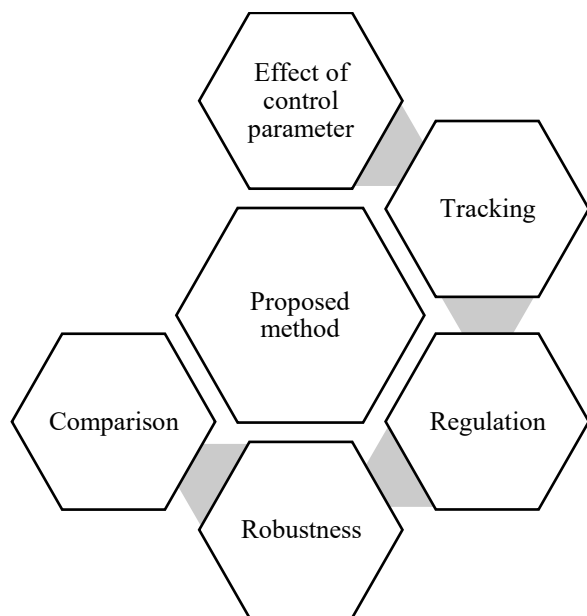


Fig. 28. Key results of the proposed method

The proposed method can be applied to other power electronic systems and converters where cascaded control structure is required to ensure input power and output energy in the desired operating region. The proposed control method can be applied to other switch-mode DC-DC converters such as buck, buck-boost, cuk, and sepic converters. Additionally, for controlling isolated DC-DC converters, this method can be employed. Improved control of DC-DC power converters will assist in the more efficient utilization of renewable energy sources. Then, it contributes to new knowledge in the domain.

One of the future works is to perform a model-based analysis (continuous or discrete) of the studied system. By utilizing a model, the Jacobian matrix can be computed. Then, by examining the eigenvalues of this matrix, stability analysis can be provided.

To overcome the high number of sensors, some variables can be estimated for further improving the control scheme. Another potential future research is integration with renewable energy sources.

ACKNOWLEDGMENT

This work was supported in part by an International Research Partnership "Electrical Engineering – Thai French Research Center (EE-TFRC)" under the project framework of the Lorraine Université d'Excellence (LUE) in cooperation

between Université de Lorraine and King Mongkut's University of Technology North Bangkok and in part by Shahid Beheshti G.C. University and was funded by National Science, Research and Innovation Fund (NSRF), and King Mongkut's University of Technology North Bangkok with Contract no. KMUTNB-FF-66-45.

REFERENCES

- [1] P. Azer and A. Emadi, "Generalized State Space Average Model for Multi-Phase Interleaved Buck, Boost and Buck-Boost DC-DC Converters: Transient, Steady-State and Switching Dynamics," in *IEEE Access*, vol. 8, pp. 77735-77745, 2020, doi: 10.1109/ACCESS.2020.2987277.
- [2] G. Spiazzi, "Analysis and design of the soft-switched clamped-resonant interleaved boost converter," *CPSS Transactions on Power Electronics and Applications*, vol. 4, no. 4, pp. 276-287, Dec. 2019.
- [3] K. A. Singh, A. Prajapati, and K. Chaudhary, "High-Gain Compact Interleaved Boost Converter With Reduced Voltage Stress for PV Application," in *IEEE Journal of Emerging and Selected Topics in Power Electronics*, vol. 10, no. 4, pp. 4763-4770, Aug. 2022, doi: 10.1109/JESTPE.2021.3120802.
- [4] W. Jiang, S. H. Chincholkar, and C. -Y. Chan, "Investigation of a Voltage-Mode Controller for a dc-dc Multilevel Boost Converter," in *IEEE Transactions on Circuits and Systems II: Express Briefs*, vol. 65, no. 7, pp. 908-912, July 2018, doi: 10.1109/TCSII.2017.2723660.
- [5] S. -W. Lee and H. -L. Do, "High Step-Up Coupled-Inductor Cascade Boost DC-DC Converter With Lossless Passive Snubber," in *IEEE Transactions on Industrial Electronics*, vol. 65, no. 10, pp. 7753-7761, Oct. 2018, doi: 10.1109/TIE.2018.2803731.
- [6] J. Kashiwagi, A. Yamaguchi, Y. Moriyama, and K. Nakahara, "Hysteretic Control Embedded Boost Converter Operating at 25-MHz Switching," in *IEEE Transactions on Circuits and Systems II: Express Briefs*, vol. 66, no. 1, pp. 101-105, Jan. 2019, doi: 10.1109/TCSII.2018.2834571.
- [7] W. Zhang, B. Zhang, and S. Li, "A Wide-Stable-Region Logarithm-Type Slope Compensation for Peak-Current-Mode Controlled Boost Converter," in *IEEE Transactions on Circuits and Systems II: Express Briefs*, vol. 69, no. 6, pp. 2927-2931, June 2022, doi: 10.1109/TCSII.2022.3153526.
- [8] S. H. Chincholkar, W. Jiang, and C. -Y. Chan, "A Modified Hysteresis-Modulation-Based Sliding Mode Control for Improved Performance in Hybrid DC-DC Boost Converter," in *IEEE Transactions on Circuits and Systems II: Express Briefs*, vol. 65, no. 11, pp. 1683-1687, Nov. 2018, doi: 10.1109/TCSII.2017.2784549.
- [9] S. H. Chincholkar, W. Jiang, and C. -Y. Chan, "An Improved PWM-Based Sliding-Mode Controller for a DC-DC Cascade Boost Converter," in *IEEE Transactions on Circuits and Systems II: Express Briefs*, vol. 65, no. 11, pp. 1639-1643, Nov. 2018, doi: 10.1109/TCSII.2017.2754292.
- [10] S. K. Pandey, S. L. Patil, U. M. Chaskar, and S. B. Phadke, "State and Disturbance Observer-Based Integral Sliding Mode Controlled Boost DC-DC Converters," in *IEEE Transactions on Circuits and Systems II: Express Briefs*, vol. 66, no. 9, pp. 1567-1571, Sept. 2019, doi: 10.1109/TCSII.2018.2888570.
- [11] V. K. Goyal and A. Shukla, "Isolated DC-DC Boost Converter for Wide Input Voltage Range and Wide Load Range Applications," in *IEEE Transactions on Industrial Electronics*, vol. 68, no. 10, pp. 9527-9539, Oct. 2021, doi: 10.1109/TIE.2020.3029479.
- [12] V. K. Goyal and A. Shukla, "Two-Stage Hybrid Isolated DC-DC Boost Converter for High Power and Wide Input Voltage Range Applications," in *IEEE Transactions on Industrial Electronics*, vol. 69, no. 7, pp. 6751-6763, July 2022, doi: 10.1109/TIE.2021.3099245.
- [13] B. Chandrasekar *et al.*, "Non-Isolated High-Gain Triple Port DC-DC Buck-Boost Converter With Positive Output Voltage for Photovoltaic Applications," in *IEEE Access*, vol. 8, pp. 113649-113666, 2020, doi: 10.1109/ACCESS.2020.3003192.
- [14] J. Liu, K. Wang, Z. Zheng, C. Li, and Y. Li, "A Dual-Active-Clamp Quasi-Resonant Isolated Boost Converter for PV Integration to Medium-Voltage DC Grids," in *IEEE Journal of Emerging and Selected Topics in Power Electronics*, vol. 8, no. 4, pp. 3444-3456, Dec. 2020, doi: 10.1109/JESTPE.2019.2924145.

- [15] M. S. Bhaskar, D. J. Almkhles, S. Padmanaban, F. Blaabjerg, U. Subramaniam, and D. M. Ionel, "Analysis and Investigation of Hybrid DC–DC Non-Isolated and Non-Inverting Nx Interleaved Multilevel Boost Converter (Nx-IMBC) for High Voltage Step-Up Applications: Hardware Implementation," in *IEEE Access*, vol. 8, pp. 87309-87328, 2020, doi: 10.1109/ACCESS.2020.2992447.
- [16] A. Iqbal, M. Sagar Bhaskar, M. Meraj and S. Padmanaban, "DC-Transformer Modelling, Analysis and Comparison of the Experimental Investigation of a Non-Inverting and Non-Isolated Nx Multilevel Boost Converter (Nx MBC) for Low to High DC Voltage Applications," in *IEEE Access*, vol. 6, pp. 70935-70951, 2018, doi: 10.1109/ACCESS.2018.2881391.
- [17] V. Seshagiri Rao and K. Sundaramoorthy, "Performance Analysis of Voltage Multiplier Coupled Cascaded Boost Converter With Solar PV Integration for DC Microgrid Application," in *IEEE Transactions on Industry Applications*, vol. 59, no. 1, pp. 1013-1023, Jan.-Feb. 2023, doi: 10.1109/TIA.2022.3209616.
- [18] A. Gupta, N. Korada, and R. Ayyanar, "Quadratic Extended-Duty-Ratio Boost Converter for Ultra High Gain Application with Low Device Stress," *2021 IEEE Applied Power Electronics Conference and Exposition (APEC)*, pp. 1796-1802, 2021, doi: 10.1109/APEC42165.2021.9487175.
- [19] N. Subhani, Z. May, M. K. Alam, I. Khan, M. A. Hossain, and S. Mamun, "An Improved Non-Isolated Quadratic DC-DC Boost Converter With Ultra High Gain Ability," in *IEEE Access*, vol. 11, pp. 11350-11363, 2023, doi: 10.1109/ACCESS.2023.3241863.
- [20] J. Roy, A. Gupta, and R. Ayyanar, "Discontinuous Conduction Mode Analysis of High Gain Extended-Duty-Ratio Boost Converter," in *IEEE Open Journal of the Industrial Electronics Society*, vol. 2, pp. 372-387, 2021, doi: 10.1109/OJIES.2021.3077982.
- [21] S. S. Sayed and A. M. Massoud, "Review on State-of-the-Art Unidirectional Non-Isolated Power Factor Correction Converters for Short-/Long-Distance Electric Vehicles," in *IEEE Access*, vol. 10, pp. 11308-11340, 2022, doi: 10.1109/ACCESS.2022.3146410.
- [22] Y. Li, F. Li, F. -W. Zhao, X. -J. You, K. Zhang, and M. Liang, "Hybrid Three-Level Full-Bridge Isolated Buck-Boost Converter With Clamped Inductor for Wider Voltage Range Application," in *IEEE Transactions on Power Electronics*, vol. 34, no. 3, pp. 2923-2937, March 2019, doi: 10.1109/TPEL.2018.2845308.
- [23] F. Wu, Z. Wang, and S. Luo, "Buck-Boost Three-Level Semi-Dual-Bridge Resonant Isolated DC-DC Converter," in *IEEE Journal of Emerging and Selected Topics in Power Electronics*, vol. 9, no. 5, pp. 5986-5995, Oct. 2021, doi: 10.1109/JESTPE.2020.3041094.
- [24] F. Wu, K. Wang, and S. Luo, "Hybrid-Three-Level Current-Fed Series-Resonant Isolated DC-DC Converter and its Optimization Modulation Strategy," in *IEEE Transactions on Power Electronics*, vol. 37, no. 1, pp. 196-205, Jan. 2022, doi: 10.1109/TPEL.2021.3098452.
- [25] C. Kang, W. Wang, W. Li, H. Du, and L. Diao, "Balance Midpoint Potential Control of Three-Level Boost Converter for Rail Transit Application," in *IEEE Access*, vol. 7, pp. 47737-47746, 2019, doi: 10.1109/ACCESS.2019.2909131.
- [26] I. A. Ayad *et al.*, "Optimized Nonlinear Integral Backstepping Controller for DC-DC Three-Level Boost Converters," in *IEEE Access*, vol. 11, pp. 49794-49805, 2023, doi: 10.1109/ACCESS.2023.3274773.
- [27] D. Luo, Y. Gao, and P. K. T. Mok, "A GaN Driver for a Bi-Directional Buck/Boost Converter With Three-Level VGS Protection and Optimal-Point Tracking Dead-Time Control," in *IEEE Transactions on Circuits and Systems I: Regular Papers*, vol. 69, no. 5, pp. 2212-2224, May 2022, doi: 10.1109/TCSI.2022.3146190.
- [28] M. G. Judewicz, S. A. González, E. M. Gelos, J. R. Fischer, and D. O. Carrica, "Exact Feedback Linearization Control of Three-Level Boost Converters," in *IEEE Transactions on Industrial Electronics*, vol. 70, no. 2, pp. 1916-1926, Feb. 2023, doi: 10.1109/TIE.2022.3158015.
- [29] N. Rana, M. Kumar, A. Ghosh, and S. Banerjee, "A Novel Interleaved Tri-State Boost Converter With Lower Ripple and Improved Dynamic Response," in *IEEE Transactions on Industrial Electronics*, vol. 65, no. 7, pp. 5456-5465, July 2018, doi: 10.1109/TIE.2017.2774775.
- [30] N. Rana, S. Banerjee, S. K. Giri, A. Trivedi, and S. S. Williamson, "Modeling, Analysis and Implementation of an Improved Interleaved Buck-Boost Converter," in *IEEE Transactions on Circuits and Systems II: Express Briefs*, vol. 68, no. 7, pp. 2588-2592, July 2021, doi: 10.1109/TCSII.2021.3056478.
- [31] S. V. Malge, M. G. Ghogare, S. L. Patil, A. S. Deshpande, and S. K. Pandey, "Chatter-Free Non-Singular Fast Terminal Sliding Mode Control of Interleaved Boost Converter," in *IEEE Transactions on Circuits and Systems II: Express Briefs*, vol. 70, no. 1, pp. 186-190, Jan. 2023, doi: 10.1109/TCSII.2022.3201959.
- [32] J. A. Morales-Saldana, E. E. C. Gutierrez, and J. Leyva-Ramos, "Modeling of switch-mode dc-dc cascade converters," in *IEEE Transactions on Aerospace and Electronic Systems*, vol. 38, no. 1, pp. 295-299, Jan. 2002, doi: 10.1109/7.993249.
- [33] G. Spiazzi and S. Buso, "An Isolated Soft-Switched High-Power-Factor Rectifier Based on the Asymmetrical Half-Bridge Flyback Converter," in *IEEE Transactions on Industrial Electronics*, vol. 69, no. 7, pp. 6722-6731, July 2022, doi: 10.1109/TIE.2021.3100975.
- [34] P. Upadhyay and R. Kumar, "A high gain cascaded boost converter with reduced voltage stress for PV application," *Solar Energy*, vol. 183, pp. 829-841, 2019.
- [35] S. Chincholkar, W. Jiang, C. Y. Chan, and S. Rangarajan, "A simplified output feedback controller for the DC-DC boost power converter," *Electronics*, vol. 10, no. 4, p. 493, 2021.
- [36] S. -W. Lee and H. -L. Do, "Quadratic Boost DC-DC Converter With High Voltage Gain and Reduced Voltage Stresses," in *IEEE Transactions on Power Electronics*, vol. 34, no. 3, pp. 2397-2404, March 2019, doi: 10.1109/TPEL.2018.2842051.
- [37] Z. Shahrouei, M. Rahmati, R. Gavagsaz-Ghoachani, M. Phattanasak, J. -P. Martin, and S. Pierfederici, "Robust Flatness-Based Control With Nonlinear Observer for Boost Converters," in *IEEE Transactions on Transportation Electrification*, vol. 9, no. 1, pp. 142-155, March 2023, doi: 10.1109/TTE.2022.3192217.
- [38] Z. Guo, H. Li, C. Liu, Y. Zhao, and W. Su, "Stability-improvement method of cascaded DC-DC converters with additional voltage-error mutual feedback control," in *Chinese Journal of Electrical Engineering*, vol. 5, no. 2, pp. 63-71, June 2019, doi: 10.23919/CJEE.2019.000012.
- [39] N. Mukherjee and D. Strickland, "Control of Cascaded DC-DC Converter-Based Hybrid Battery Energy Storage Systems—Part II: Lyapunov Approach," in *IEEE Transactions on Industrial Electronics*, vol. 63, no. 5, pp. 3050-3059, May 2016, doi: 10.1109/TIE.2015.2511159.
- [40] L. V. Bellinaso, H. H. Figueira, M. F. Basquera, R. P. Vieira, H. A. Gründling, and L. Michels, "Cascade Control With Adaptive Voltage Controller Applied to Photovoltaic Boost Converters," in *IEEE Transactions on Industry Applications*, vol. 55, no. 2, pp. 1903-1912, March-April 2019, doi: 10.1109/TIA.2018.2884904.
- [41] S. M. Rakhtala and A. Casavola, "Real-Time Voltage Control Based on a Cascaded Super Twisting Algorithm Structure for DC-DC Converters," in *IEEE Transactions on Industrial Electronics*, vol. 69, no. 1, pp. 633-641, Jan. 2022, doi: 10.1109/TIE.2021.3051551.
- [42] M. Afkar, R. Gavagsaz-Ghoachani, M. Phattanasak, and S. Pierfederici, "Cascaded Controller for Controlling DC Bus Voltage in Mismatched Input Powers," in *IEEE Transactions on Power Electronics*, vol. 37, no. 11, pp. 13834-13847, Nov. 2022, doi: 10.1109/TPEL.2022.3186233.
- [43] R. Gavagsaz-Ghoachani, M. Phattanasak, J. -P. Martin, B. Nahid-Mobarakeh, and S. Pierfederici, "A Fixed-Frequency Optimization of PWM Current Controller—Modeling and Design of Control Parameters," in *IEEE Transactions on Transportation Electrification*, vol. 4, no. 3, pp. 671-683, Sept. 2018, doi: 10.1109/TTE.2018.2841801.
- [44] M. E. Albira and M. A. Zohdy, "Adaptive Model Predictive Control for DC-DC Power Converters With Parameters' Uncertainties," in *IEEE Access*, vol. 9, pp. 135121-135131, 2021, doi: 10.1109/ACCESS.2021.3113299.
- [45] A. Sureshkumar and R. Gunabalan, "Design of Robust Guaranteed Margin Stability Region PI Controller for Automotive LED Lighting With Parameter Uncertainty," in *IEEE Access*, vol. 10, pp. 15657-15670, 2022, doi: 10.1109/ACCESS.2022.3146392.
- [46] J. Liu, "Impedance Analysis of Battery Bidirectional DC-DC Converter," in *IEEE Access*, vol. 8, pp. 30960-30968, 2020, doi: 10.1109/ACCESS.2020.2972647.
- [47] M. Leng, G. Zhou, Q. Tian, G. Xu, and F. Blaabjerg, "Small Signal Modeling and Design Analysis for Boost Converter With Valley V2

- Control," in *IEEE Transactions on Power Electronics*, vol. 35, no. 12, pp. 13475-13487, Dec. 2020, doi: 10.1109/TPEL.2020.2990305.
- [48] I. Biswas, D. Kastha, and P. Bajpai, "Small Signal Modeling and Decoupled Controller Design for a Triple Active Bridge Multiport DC-DC Converter," in *IEEE Transactions on Power Electronics*, vol. 36, no. 2, pp. 1856-1869, Feb. 2021, doi: 10.1109/TPEL.2020.3006782.
- [49] Q. Xu, N. Vafamand, L. Chen, T. Dragičević, L. Xie, and F. Blaabjerg, "Review on Advanced Control Technologies for Bidirectional DC/DC Converters in DC Microgrids," in *IEEE Journal of Emerging and Selected Topics in Power Electronics*, vol. 9, no. 2, pp. 1205-1221, April 2021, doi: 10.1109/JESTPE.2020.2978064.
- [50] C. Yanarates and Z. Zhou, "Design and Cascade PI Controller-Based Robust Model Reference Adaptive Control of DC-DC Boost Converter," *IEEE Access*, vol. 10, pp. 44909-44922, April 2022, doi: 10.1109/ACCESS.2022.3169591.
- [51] M. Afkar, R. Gavagsaz-Ghoachani, M. Phattanasak, and S. Pierfederici, "Operating Mode Analysis of a Modular Converter: Experimental Validation," in *IEEE Transactions on Industry Applications*, vol. 58, no. 4, pp. 4889-4902, July-Aug. 2022, doi: 10.1109/TIA.2022.3171527.
- [52] H. Komurcugil, S. Biricik, and N. Guler, "Indirect Sliding Mode Control for DC-DC SEPIC Converters," in *IEEE Transactions on Industrial Informatics*, vol. 16, no. 6, pp. 4099-4108, June 2020, doi: 10.1109/TII.2019.2960067.
- [53] M. Gao, D. Wang, Y. Li, and T. Yuan, "Fixed Frequency Pulse-Width Modulation Based Integrated Sliding Mode Controller for Phase-Shifted Full-Bridge Converters," in *IEEE Access*, vol. 6, pp. 2181-2192, 2018, doi: 10.1109/ACCESS.2017.2782225.
- [54] J. Slotine, W. Li., Applied Nonlinear Control, Taiwan Prentice Hall, 1991.
- [55] M. P. Aghababa, "Stabilization of Canonical Systems via Adaptive Chattering Free Sliding Modes With No Singularity Problems," in *IEEE Transactions on Systems, Man, and Cybernetics: Systems*, vol. 50, no. 5, pp. 1696-1703, May 2020, doi: 10.1109/TSMC.2017.2782767.
- [56] M. Afkar, R. Gavagsaz-Ghoachani, M. Phattanasak, J. -P. Martin, and S. Pierfederici, "Proposed System Based on a Three-Level Boost Converter to Mitigate Voltage Imbalance in Photovoltaic Power Generation Systems," in *IEEE Transactions on Power Electronics*, vol. 37, no. 2, pp. 2264-2282, Feb. 2022, doi: 10.1109/TPEL.2021.3105571.
- [57] A. Shahin, M. Hinaje, J. -P. Martin, S. Pierfederici, S. Rael, and B. Davat, "High Voltage Ratio DC-DC Converter for Fuel-Cell Applications," in *IEEE Transactions on Industrial Electronics*, vol. 57, no. 12, pp. 3944-3955, Dec. 2010, doi: 10.1109/TIE.2010.2045996.
- [58] M. Afkar, R. Gavagsaz-Ghoachani, M. Phattanasak, A. Siangsanoh, J. -P. Martin, and S. Pierfederici, "Generalization of a DC-DC Modular Converter Topology for Fuel Cell Applications," in *IEEE Transactions on Industry Applications*, vol. 58, no. 2, pp. 2255-2267, March-April 2022, doi: 10.1109/TIA.2022.3142659.
- [59] M. Afkar, R. Gavagsaz-Ghoachani, M. Phattanasak, and S. Pierfederici, "Commandable areas of a modular converter for DC voltage imbalance mitigation in fuel cell systems," *Sustain. Energy Technol. Assess.*, vol. 48, p. 101664, Dec. 2021.
- [60] R. Gavagsaz-Ghoachani, L.-M. Saublet, M. Phattanasak, J.-P. Martin, B. Nahid-mobarakeh, S. Pierfederici, "Active stabilization design of DC-DC converters with constant power load using a sampled discrete-time model: stability analysis and experimental verification," *IET Power Electron.*, vol. 11, pp. 1519-1528, 2018.
- [61] R. Gavagsaz-Ghoachani, M. Phattanasak, J. P. Martin, and S. Pierfederici, "Lyapunov function-based improved switching command for a boost converter with an inductor-capacitor input filter," *IET Power Electronics*, vol. 13, no. 17, pp. 3940-3953, 2020.
- [62] R. Gavagsaz-Ghoachani, M. Phattanasak, J. -P. Martin, B. Nahid-Mobarakeh, S. Pierfederici, and P. Riedinger, "Observer and Lyapunov-Based Control for Switching Power Converters With LC Input Filter," in *IEEE Transactions on Power Electronics*, vol. 34, no. 7, pp. 7053-7066, July 2019, doi: 10.1109/TPEL.2018.2877180.
- [63] M. Rasouli, M. Mehra, A. Ganjavi, M. S. Sadabadi, H. Ghoreishy, and A. Ale Ahmad, "Lyapunov-Based Control Strategy for a Single-Input Dual-Output Three-Level DC/DC Converter," in *IEEE Transactions on Industrial Electronics*, vol. 70, no. 10, pp. 10486-10495, Oct. 2023, doi: 10.1109/TIE.2022.3217610.
- [64] W. Ma, B. Zhang, D. Qiu, and H. Sun, "Switching Control Strategy for DC-DC Converters Based on Polynomial Lyapunov Function and Sum-of-Squares Approach," in *IEEE Transactions on Industrial Electronics*, vol. 70, no. 4, pp. 3663-3673, April 2023, doi: 10.1109/TIE.2022.3179548.
- [65] A. Lekić, D. Stipanović, and N. Petrović, "Controlling the Čuk Converter Using Polytopic Lyapunov Functions," in *IEEE Transactions on Circuits and Systems II: Express Briefs*, vol. 65, no. 11, pp. 1678-1682, Nov. 2018, doi: 10.1109/TCSII.2017.2781621.
- [66] r. Silva-Ortigoza *et al.*, "Hierarchical Flatness-Based Control for Velocity Trajectory Tracking of the "DC/DC Boost Converter-DC Motor" System Powered by Renewable Energy," in *IEEE Access*, vol. 11, pp. 32464-32475, 2023, doi: 10.1109/ACCESS.2023.3260188.
- [67] J. R. García-Sánchez *et al.*, "A Robust Differential Flatness-Based Tracking Control for the "MIMO DC/DC Boost Converter-Inverter-DC Motor" System: Experimental Results," in *IEEE Access*, vol. 7, pp. 84497-84505, 2019, doi: 10.1109/ACCESS.2019.2923701.
- [68] L. Gil-Antonio, B. Saldívar, O. Portillo-Rodríguez, G. Vázquez-Guzmán, and S. M. De Oca-Armeaga, "Trajectory Tracking Control for a Boost Converter Based on the Differential Flatness Property," in *IEEE Access*, vol. 7, pp. 63437-63446, 2019, doi: 10.1109/ACCESS.2019.2916472.
- [69] Y. Huangfu, Q. Li, L. Xu, R. Ma, and F. Gao, "Extended State Observer Based Flatness Control for Fuel Cell Output Series Interleaved Boost Converter," in *IEEE Transactions on Industry Applications*, vol. 55, no. 6, pp. 6427-6437, Nov.-Dec. 2019, doi: 10.1109/TIA.2019.2936331.
- [70] M. Zauner, P. Mandl, C. Hametner, O. König, and S. Jakubek, "Flatness-Based Discrete-Time Control of a Battery Emulator Driving a Constant Power Load," in *IEEE Journal of Emerging and Selected Topics in Power Electronics*, vol. 9, no. 6, pp. 6864-6874, Dec. 2021, doi: 10.1109/JESTPE.2021.3059917.
- [71] S. J. Yaqoob *et al.*, "Efficient Flatness Based Energy Management Strategy for Hybrid Supercapacitor/Lithium-ion Battery Power System," in *IEEE Access*, vol. 10, pp. 132153-132163, 2022, doi: 10.1109/ACCESS.2022.3230333.
- [72] A. Siangsanoh *et al.*, "Hybrid Fuel Cell/Supercapacitor using a Series Converter," 2019 IEEE Energy Conversion Congress and Exposition (ECCE), pp. 6711-6716, 2019, doi: 10.1109/ECCE.2019.8912658.
- [73] B. Brahmī *et al.*, "Flatness Based Control of a Novel Smart Exoskeleton Robot," in *IEEE/ASME Transactions on Mechatronics*, vol. 27, no. 2, pp. 974-984, April 2022, doi: 10.1109/TMECH.2021.3076956.
- [74] T. Turahyo, "A simple strategy of control dc-dc converter as power supply on household lights," *Journal of Robotics and Control (JRC)*, vol. 2, no. 6, pp. 484-488, Nov 2021.
- [75] M. Bahrāmī, R. Gavagsaz-Ghoachani, M. Zandi, M. Phattanasak, Gaël Maranzana, B. Nahid-Mobarakeh, S. Pierfederici, and F. Meibody-Tabar, "Hybrid maximum power point tracking algorithm with improved dynamic performance," *Renewable Energy*, vol. 130, pp. 982-991, Jan 2019.
- [76] B. Babes, S. Mekhilef, A. Boutaghane, and L. Rahmani, "Fuzzy Approximation-Based Fractional-Order Nonsingular Terminal Sliding Mode Controller for DC-DC Buck Converters," in *IEEE Transactions on Power Electronics*, vol. 37, no. 3, pp. 2749-2760, March 2022, doi: 10.1109/TPEL.2021.3114277.
- [77] H. K. Khalil, *Nonlinear Systems*. 3rd Edition, Prentice Hall, Upper Saddle River, 2002.
- [78] Y. Zou, L. Zhang, J. Qin, W. Sheng, and Q. Duan, "Phase-Unsynchronized Power Decoupling Control of MMC Based on Feedback Linearization," in *IEEE Transactions on Power Electronics*, vol. 37, no. 3, pp. 2946-2958, March 2022, doi: 10.1109/TPEL.2021.3119527.
- [79] H. Li, Z. Wang, Z. Xu, X. Wang, and Y. Hu, "Feedback Linearization Based Direct Torque Control for IPMSMs," in *IEEE Transactions on Power Electronics*, vol. 36, no. 3, pp. 3135-3148, March 2021, doi: 10.1109/TPEL.2020.3012107.
- [80] M. Phattanasak, R. Gavagsaz-Ghoachani, J. -P. Martin, B. Nahid-Mobarakeh, S. Pierfederici, and B. Davat, "Control of a Hybrid Energy Source Comprising a Fuel Cell and Two Storage Devices Using

- Isolated Three-Port Bidirectional DC–DC Converters," in *IEEE Transactions on Industry Applications*, vol. 51, no. 1, pp. 491-497, Jan.-Feb. 2015, doi: 10.1109/TIA.2014.2336975.
- [81] D. Dell'Isola, M. Urbain, M. Weber, S. Pierfederici, and F. Meibody-Tabar, "Optimal Design of a DC–DC Boost Converter in Load Transient Conditions, Including Control Strategy and Stability Constraint," in *IEEE Transactions on Transportation Electrification*, vol. 5, no. 4, pp. 1214-1224, Dec. 2019, doi: 10.1109/TTE.2019.2948038.
- [82] M. R. Banaei and H. A. F. Bonab, "A High Efficiency Nonisolated Buck–Boost Converter Based on ZETA Converter," in *IEEE Transactions on Industrial Electronics*, vol. 67, no. 3, pp. 1991-1998, March 2020, doi: 10.1109/TIE.2019.2902785.
- [83] M. Najjar, A. Kouchaki, J. Nielsen, R. Dan Lazar, and M. Nymand, "Design Procedure and Efficiency Analysis of a 99.3% Efficient 10 kW Three-Phase Three-Level Hybrid GaN/Si Active Neutral Point Clamped Converter," in *IEEE Transactions on Power Electronics*, vol. 37, no. 6, pp. 6698-6710, June 2022, doi: 10.1109/TPEL.2021.3131955.